ELSEVIER

Int. J. Therm. Sci. 41 (2002) 500–508

International Journal of Thermal Sciences

www.elsevier.com/locate/ijts

Three-dimensional modelling and optimisation of thermal fields induced in a human body during hyperthermia ☆

Cédric Thiebaut *, Denis Lemonnier

Laboratoire d'Études Thermiques, UMR CNRS 6608, ENSMA-BP 40109, 86961 Futuroscope Chasseneuil cedex, France

Received 19 September 2001; accepted 20 March 2002

Abstract

In the field of hyperthermia as a cancer therapy, the design of tools to predict as well as to control the thermal fields in biological tissues remains a task of highest importance. In this context, we have developed a three-dimensional numerical model in heterogeneous media in order to compute the rate of volumetric heat generation, produced by means of an electromagnetic irradiation, and the resulting temperature distribution. The electromagnetic power deposition within the tissues is predicted by solving the Maxwell's field equations in the frequency-domain and the thermal process is described by the Pennes' bio-heat transfer equation. All the governing equations have been solved using the boundary element method. Furthermore, our simulation tool has been coupled to an optimisation procedure, whose parameters are the amplitude and phase of each electromagnetic source. The objective is to achieve the highest possible temperature in the tumour without exceeding 42 °C in the surrounding healthy tissues. Simulations based on a three-dimensional heterogeneous model constructed from cross-sectional slices of a person are presented. The studied configurations concern the pelvic region where a tumour is deeply embedded. The efficiency of our optimisation routine in a treatment plan for regional hyperthermia is reported.

Keywords: Thermotherapy; Electromagnetic heating; Bio-heat transfer; Boundary element method; Treatment planning

1. Introduction

Hyperthermia—increase of biological tissues temperature—has become a useful form of cancer therapy. Based on antitumoral properties of heat, it can be applied either alone, or in conjunction with radiotherapy and/or chemotherapy. Hyperthermia treatment aims at achieving a therapeutic temperature elevation in tumour tissue (greater than 42 °C) without exceeding the normal physiologic range in healthy tissues (lower than 42 °C). Several hyperthermia delivery systems can be used; it depends on the tumour localisation. Local heating may be generated either invasively, e.g., by small microwave antennae inserted into the tumour through hypodermic needles, or noninvasively by ultrasound transducers for superficial tumours. Regional heating by electromagnetic waves may be produced noninvasively for deep-seated tumours with different types of applicators working at radio frequency: magnetic induction devices, waveguides, antennae and capacitive plates. It should be underlined here that deep heating commonly involves multiapplicator devices which consist of phased arrays of electromagnetic sources. Furthermore, if a suitable arrangement of source amplitude and phase is used, it is possible to improve the focalisation of the heat deposition in the tumour volume [1]. However, the effective and efficient use of this therapy under clinical routine conditions is still limited, especially because of the lack of knowledge of the heating patterns. Indeed, an excessive temperature in healthy tissues ("hot spots") leads to pain episodes. Moreover, due to patient tolerance considerations, only a few thermometers can be inserted into the body (typically a maximum of 4 to 5). Consequently, detailed thermal measurements are presently impractical, particularly for deep-seated tumours. Thus, numerical modelling appears to be a useful tool for both temperature prediction and control within the scope of hyperthermia treatment plan [2–5].

☆ This article is a follow up a communication presented by the authors at the EUROTHERM Seminar 68, "Inverse problems and experimental design in thermal and mechanical engineering", held in Poitiers in March 2001.

* Correspondence and reprints.

E-mail addresses: cedric.thiebaut@let.ensma.fr (C. Thiebaut), lemonnier@let.ensma.fr (D. Lemonnier).

1290-0729/02/$ – see front matter
PII: S1290-0729(02)01343-1

Nomenclature

C_{pb}	specific heat of blood	$J \cdot kg^{-1} \cdot K^{-1}$
$\boldsymbol{E}$	complex electric field vector	$V \cdot m^{-1}$
F	objective function	°C
g	constraint function	°C
G	fundamental solution	
$\boldsymbol{H}$	complex magnetic field vector	$A \cdot m^{-1}$
i	unit imaginary number	
$\boldsymbol{n}$	normal unit vector	
N	number of electromagnetic sources	
N_C	number of control points	
Q_{wave}	electromagnetic power deposition	$W \cdot m^{-3}$
Q_m	metabolic power deposition	$W \cdot m^{-3}$
T	temperature of tissue	°C
T_a	temperature of arterial blood	°C
W_b	volumetric perfusion rate	$kg \cdot m^{-3} \cdot s^{-1}$
$\boldsymbol{x}$	position vector	m
$\boldsymbol{x}_M$	position vector of optimisation point	m
$\boldsymbol{x}_C$	position vector of control point	m
Z	complex amplitude	

Greek symbols

α	real part of Z	
β	imaginary part of Z	
δ	Dirac delta function	
ε	electrical permittivity	$F \cdot m^{-1}$
ε^*	complex permittivity	$F \cdot m^{-1}$
Φ	solid angle	sr
Γ	boundary of Ω	
κ	complex wave number	m^{-1}
λ	thermal conductivity	$W \cdot m^{-1} \cdot °C^{-1}$
σ	electrical conductivity	$S \cdot m^{-1}$
μ	magnetic permeability	$H \cdot m^{-1}$
ω	angular frequency	$rad \cdot s^{-1}$
Ω	global domain	

Subscripts

i	source point index
j	control point index
k, l	electromagnetic source indices

Superscripts

R, I	indices related to the temperature field solution of the thermal problem with a source term, respectively, equal to the real and imaginary part of a complex quantity

The problem that must be solved is by itself twofold: first, estimate the rate of power deposition in various tissues by electromagnetic irradiation, and second, calculate the resulting temperature distribution. In our code, the first stage is achieved by solving the Maxwell's field equations in complex form to compute the electric field within the tissues. The second is based on the solution of the Pennes' bio-heat transfer equation with a source term deduced from electromagnetic calculations. These two problems are treated by a three-dimensional boundary element formulation. This method is now well established and has emerged as a powerful alternative numerical technique. By transforming the original domain into a boundary integral equation form, it reduces the dimension of the problem by one and requires only a discretisation over the boundary instead of throughout the domain. Moreover, it can easily deal with infinite boundaries which occur in the electromagnetic problem.

In this paper, we present some numerical results based on a three-dimensional heterogeneous anatomical model in the field of regional hyperthermia where a large part of the body around the tumour is heated. We have simulated a commercially available multiapplicator device known as the Sigma-60 [6] (BSD Medical Corporation, Salt Lake City, Utah, USA). The selection of the amplitude and the phase of each electromagnetic source here relies on an optimisation of the temperature distribution within tissues. So far, these parameters have been mostly determined through an optimisation of the power deposition only [1,7–9]. However, due to the large effect of the blood flow on the temperature distribution in the living tissues, both an efficient and safe hyperthermia treatment is not necessarily provided.

2. Mathematical model

The bio-heat transfer equation expresses the energy balance in a volume control of perfused tissue between conductive heat transport, heat loss due to the blood flow, metabolism and energy deposition due to the hyperthermia application. In a homogeneous tissue it has the following differential form:

$$\lambda \Delta T + W_b C_{pb} (T_a - T) + Q_m + Q_{wave} = 0 \tag{1}$$

where λ is the thermal conductivity, W_b the volumetric perfusion rate, T the local temperature of tissue, C_{pb} the specific heat of blood, T_a the temperature of arterial blood, Q_m the power produced by metabolic process and Q_{wave} the electromagnetic power deposition. The boundary conditions considered are specified on the body surface and can be of two kinds: constant-temperature or convection conditions.

The spatial and temporal behaviour of the electromagnetic field within the tissues is governed by the Maxwell's equations, here written for lossy dielectric media. By

assuming a periodic time variation of the form $e^{-i\omega t}$, these equations are expressed, in a homogeneous tissue, as:

$$\begin{cases} \nabla \times \mathbf{E} = i\omega\mu\mathbf{H} \\ \nabla \cdot \mathbf{E} = 0 \\ \nabla \cdot \mathbf{H} = 0 \\ \nabla \times \mathbf{H} = -i\omega\varepsilon^*\mathbf{E} \end{cases} \tag{2}$$

where $\boldsymbol{E}$ is the complex electric field, $\boldsymbol{H}$ the complex magnetic field, ω the angular frequency, ε, σ and μ the electrical permittivity, the electrical conductivity and the magnetic permeability of tissue, respectively, and ε^* the complex permittivity defined by: $\varepsilon^* = \varepsilon + i\sigma/\omega$. The electromagnetic power deposition averaged over time is then calculated by:

$$Q_{\text{wave}} = \frac{\sigma}{2}|\mathbf{E}|^2 \tag{3}$$

Both ε and σ depend on frequency, μ being constant and equal to the free space value. At the interface separating two electrically distinct tissue types, all electromagnetic field components are continuous except for the normally directed electric field which is discontinuous and satisfies:

$$\varepsilon_1^*(\boldsymbol{n} \cdot \boldsymbol{E}_1) = \varepsilon_2^*(\boldsymbol{n} \cdot \boldsymbol{E}_2) \tag{4}$$

where the subscripts distinguish the two tissue types forming the interface and $\boldsymbol{n}$ is the unit normal vector to this interface. In this study, the boundary conditions are prescribed over the surface of each electromagnetic source where $(\boldsymbol{n} \times \boldsymbol{H})$ is presumed known.

3. Boundary element formulation

Let Ω be a homogeneous volume bounded by a surface Γ and $\boldsymbol{n}$ be the unit outward-pointing normal vector to this surface. The boundary integral formulation for the electric field is obtained from the Maxwell's equations by applying the weighted residual technique [10] and the vector Green's theorem [11]:

$$\frac{\Phi_i}{4\pi}\boldsymbol{E}_i = -\int_\Gamma \big[(\boldsymbol{n} \times \boldsymbol{E}) \times \nabla G_i + (\boldsymbol{n} \cdot \boldsymbol{E})\nabla G_i + i\omega\mu(\boldsymbol{n} \times \boldsymbol{H})G_i\big]\,dS \tag{5}$$

where Φ_i is the solid angle subtended by Γ at the point $\boldsymbol{x}_i$ and G_i is the fundamental solution of the Helmholtz's equation for the unbounded space:

$$\Delta G_i + \kappa^2 G_i = -\delta(\boldsymbol{x} - \boldsymbol{x}_i) \tag{6}$$

δ being the Dirac delta function, $\boldsymbol{x}_i$ the source point at which this function has its singularity, $\boldsymbol{x}$ the observation point which is the variable involved in our differential equations and κ the complex wave number defined by: $\kappa^2 = \omega^2\mu\varepsilon^*$. The solution of Eq. (6) in three dimensions is given by:

$$G_i(\boldsymbol{x}) = \frac{e^{i\kappa|\boldsymbol{x}-\boldsymbol{x}_i|}}{4\pi|\boldsymbol{x}-\boldsymbol{x}_i|} \tag{7}$$

Dealing with the thermal problem, Eq. (1) has first been modified into a Helmholtz's equation with a source term:

$$\Delta T - \frac{W_b C_{pb}}{\lambda}T = -\frac{1}{\lambda}(W_b C_{pb} T_a + Q_m + Q_{\text{wave}}) \tag{8}$$

From Eq. (8) the weighted residual technique, as well as the second Green's theorem, have been applied to obtain a boundary integral formulation for the temperature field:

$$\frac{\Phi_i}{4\pi}T_i = \int_\Gamma \left(G_i\frac{\partial T}{\partial n} - \frac{\partial G_i}{\partial n}T\right)dS + \int_\Omega \frac{1}{\lambda}(W_b C_{pb} T_a + Q_m + Q_{\text{wave}})G_i\,dV \tag{9}$$

where the fundamental solution G_i is still given by Eq. (7) but now with $\kappa = i\sqrt{W_b C_{pb}/\lambda}$.

Eqs. (5) and (9) have been discretised by using the boundary element method [10,12] with constant triangular elements. It should be pointed here that an integral over the whole domain Ω occurs in Eq. (9). Although it does not introduce any new unknowns, it requires the calculation of domain integrals. Some methods, which rely on a transformation of this integral into an equivalent contour form, have been developed [13]. Nevertheless, they cannot be applied in our case because the electromagnetic power deposition is only known numerically. Thus, a volumic mesh of the domain Ω, whose elements act here like integration cells, had to be constructed. At last, note that a heterogeneous medium is treated as a piecewise homogeneous domain. Thus, Eqs. (5) and (9) can be applied to each homogeneous subdomain separately.

4. Optimisation procedure

The optimisation method we developed relies on the ability to formulate explicitly the electric field, the electromagnetic power deposition and then the temperature field as functions of the parameters, amplitude and phase, of each electromagnetic source. Let us consider a multiapplicator device composed of N electromagnetic sources. By taking advantage of the linearity of the resulting electric field, the total field $\boldsymbol{E}$ at any point in space may be viewed as a superposition of the field produced by each individual source:

$$\boldsymbol{E} = \sum_{k=1}^{N} Z_k \boldsymbol{E}_k \tag{10}$$

where $\boldsymbol{E}_k$ represents the electric field computed when the source k is driven by a signal of unit amplitude and zero phase and Z_k the complex-valued amplitude for this source. From Eq. (3) the electromagnetic power deposition becomes:

$$Q_{\text{wave}} = \frac{\sigma}{2}\sum_{1\leqslant k,\ l\leqslant N} Z_k \overline{Z}_l \boldsymbol{E}_k \cdot \overline{\boldsymbol{E}}_l \tag{11}$$

where the bar symbolises the complex conjugate. Let α_k and β_k be the real and imaginary part of Z_k, respectively. Given that:

$$Z_k\overline{Z}_l\boldsymbol{E}_k\cdot\overline{\boldsymbol{E}}_l + Z_l\overline{Z}_k\boldsymbol{E}_l\cdot\overline{\boldsymbol{E}}_k = 2\,\mathrm{Re}\big(Z_k\overline{Z}_l\boldsymbol{E}_k\cdot\overline{\boldsymbol{E}}_l\big) \tag{12}$$

and that:

$$\begin{aligned}&\mathrm{Re}\big(Z_k\overline{Z}_l\boldsymbol{E}_k\cdot\overline{\boldsymbol{E}}_l\big)\\&\quad=\mathrm{Re}\big(Z_k\overline{Z}_l\big)\,\mathrm{Re}\big(\boldsymbol{E}_k\cdot\overline{\boldsymbol{E}}_l\big)-\mathrm{Im}\big(Z_k\overline{Z}_l\big)\,\mathrm{Im}\big(\boldsymbol{E}_k\cdot\overline{\boldsymbol{E}}_l\big)\end{aligned} \tag{13}$$

it follows:

$$\begin{aligned}&Z_k\overline{Z}_l\boldsymbol{E}_k\cdot\overline{\boldsymbol{E}}_l + Z_l\overline{Z}_k\boldsymbol{E}_l\cdot\overline{\boldsymbol{E}}_k\\&\quad=2\big[(\alpha_k\alpha_l+\beta_k\beta_l)\,\mathrm{Re}\big(\boldsymbol{E}_k\cdot\overline{\boldsymbol{E}}_l\big)\\&\qquad+(\alpha_k\beta_l-\beta_k\alpha_l)\,\mathrm{Im}\big(\boldsymbol{E}_k\cdot\overline{\boldsymbol{E}}_l\big)\big]\end{aligned} \tag{14}$$

where Re( ) and Im( ) denote the real and imaginary part, respectively. From Eqs. (11) and (14) it can be obtained:

$$\begin{aligned}Q_{\mathrm{wave}} = \frac{\sigma}{2}\Bigg\{&\sum_{k=1}^{N}\big(\alpha_k^2+\beta_k^2\big)|\boldsymbol{E}_k|^2\\&+2\sum_{1\leqslant k<l\leqslant N}\big[(\alpha_k\alpha_l+\beta_k\beta_l)\,\mathrm{Re}\big(\boldsymbol{E}_k\cdot\overline{\boldsymbol{E}}_l\big)\\&+(\alpha_k\beta_l-\beta_k\alpha_l)\,\mathrm{Im}\big(\boldsymbol{E}_k\cdot\overline{\boldsymbol{E}}_l\big)\big]\Bigg\}\end{aligned} \tag{15}$$

The thermal problem being linear with respect to the source term, the temperature may be expressed at any point as:

$$\begin{aligned}T = T_{(0)}&+\sum_{k=1}^{N}\big(\alpha_k^2+\beta_k^2\big)T_{k,k}\\&+\sum_{1\leqslant k<l\leqslant N}\big[(\alpha_k\alpha_l+\beta_k\beta_l)T_{k,l}^{\mathrm{R}}+(\alpha_k\beta_l-\beta_k\alpha_l)T_{k,l}^{\mathrm{I}}\big]\end{aligned} \tag{16}$$

where $T_{(0)}$, $T_{k,k}$, $T_{k,l}^{\mathrm{R}}$ and $T_{k,l}^{\mathrm{I}}$ refer to the computed temperature fields, solutions of the thermal problem with a source term equal to $W_{\mathrm{b}}C_{\mathrm{pb}}T_{\mathrm{a}}+Q_{\mathrm{m}}$, $(\sigma/2)|\boldsymbol{E}_k|^2$, $\sigma\,\mathrm{Re}(\boldsymbol{E}_k\cdot\overline{\boldsymbol{E}}_l)$ and $\sigma\,\mathrm{Im}(\boldsymbol{E}_k\cdot\overline{\boldsymbol{E}}_l)$, respectively. Therefore, the electric field and the temperature field are everywhere functions of the free variables, amplitude and phase, of each electromagnetic source. It must be emphasised here that the computation of the electric field distributions, $\boldsymbol{E}_k$, and the temperature field distributions, $T_{(0)}$, $T_{k,k}$, $T_{k,l}^{\mathrm{R}}$ and $T_{k,l}^{\mathrm{I}}$, requires one run of the code only. Afterwards, the total electric field and the total temperature field can be calculated simply by using, respectively, Eqs. (10) and (16) for any configuration of the heating device.

The expression of the temperature field has been employed to perform the evaluation of the parameters, amplitude and phase, of each electromagnetic source by means of an optimisation procedure. It consists of maximising the temperature at a point seated within the tumour volume (typically the "centre") subject to the constraint that the temperature at some points localised in the healthy tissues remains lower than 42 °C. These control points are chosen at the centres of the cells which constitute the mesh of the domain required to treat the thermal problem. Let $\boldsymbol{x}_{\mathrm{M}}$ be the centre of the tumour volume and $\boldsymbol{x}_{C_j}$ the jth of the N_{C} control points distributed within the healthy tissues. Thereby, the objective function, F, can be represented by:

$$\begin{aligned}&F(\alpha_1,\ldots,\alpha_N,\beta_1,\ldots,\beta_N)\\&\quad=T_{(0)}(\boldsymbol{x}_M)+\sum_{k=1}^{N}\big(\alpha_k^2+\beta_k^2\big)T_{k,k}(\boldsymbol{x}_M)\\&\qquad+\sum_{1\leqslant k<l\leqslant N}\big[(\alpha_k\alpha_l+\beta_k\beta_l)T_{k,l}^{\mathrm{R}}(\boldsymbol{x}_M)\\&\qquad\qquad+(\alpha_k\beta_l-\beta_k\alpha_l)T_{k,l}^{\mathrm{I}}(\boldsymbol{x}_M)\big]\end{aligned} \tag{17}$$

and the N_{C} constraint functions, g_j, by:

$$\begin{aligned}&g_j(\alpha_1,\ldots,\alpha_N,\beta_1,\ldots,\beta_N)\\&\quad=T_{(0)}(\boldsymbol{x}_{C_j})+\sum_{k=1}^{N}\big(\alpha_k^2+\beta_k^2\big)T_{k,k}(\boldsymbol{x}_{C_j})\\&\qquad+\sum_{1\leqslant k<l\leqslant N}\big[(\alpha_k\alpha_l+\beta_k\beta_l)T_{k,l}^{\mathrm{R}}(\boldsymbol{x}_{C_j})\\&\qquad\qquad+(\alpha_k\beta_l-\beta_k\alpha_l)T_{k,l}^{\mathrm{I}}(\boldsymbol{x}_{C_j})\big]\end{aligned} \tag{18}$$

Consequently, the optimisation problem is mathematically stated as:

$$\text{Maximise } F(\alpha_1,\ldots,\alpha_N,\beta_1,\ldots,\beta_N) \tag{19}$$

subject to

$$g_j(\alpha_1,\ldots,\alpha_N,\beta_1,\ldots,\beta_N)\leqslant 42\,^{\circ}\mathrm{C},\quad j=1,\ldots,N_{\mathrm{C}} \tag{20}$$

This problem, which involves the maximisation of a non-linear function subject to a set of non-linear constraint functions, has been solved by means of the E04UCF routine from the NAG library. It is based on a sequential quadratic programming algorithm (SQP).

5. Results

To show the capabilities of our simulation and optimisation tool we have performed some calculations based on a three-dimensional heterogeneous model constructed from cross-sectional slices of a person. The part of the anatomy and the internal structures which were modelled, as well as their boundary element grid, are indicated in Fig. 1. The tumour mass is deeply embedded in the pelvic region, which represents a typical case in the deep hyperthermia context. We have simulated the Sigma-60 multiapplicator device. Designed for deep heating, it consists of eight dipole-like antennas, which are evenly spaced around an annulus encompassing the patient. Along the longitudinal length of each antenna, we specified a surface current distribution which is sinusoidal in space. This distribution peaks at the

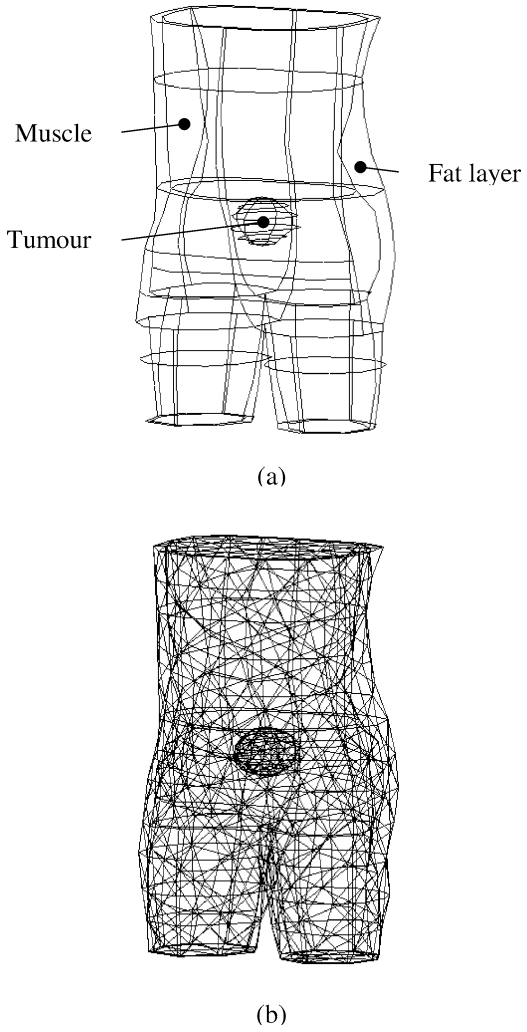

Fig. 1. (a) Three-dimensional sketch of the pelvic model, and (b) its boundary element computational grid.

antenna centre and vanishes at its two ends. The space between the sources and the body is filled by a bolus which contains some deionised water at 10 °C. The bolus improves the cooling of the skin and the electromagnetic coupling between the body and the sources. Temperature is prescribed at 10 °C on the skin area in contact with the bolus. On the other areas, we describe the heat flow to the surroundings by convective heat transfer, the heat transfer coefficient being set to 10 $W{\cdot}m^{-2}{\cdot}{}^{\circ}C^{-1}$ and the ambient temperature to 20 °C. The background medium, which is treated as an infinite domain, is air. A view of the pelvic model enclosed within this electromagnetic applicator is displayed in Fig. 2.

In this study, we assume that the amplitude and phase of each antenna can be separately chosen. The frequency of excitation is set to 100 MHz. The different values for the electrical, thermal and thermophysical properties of the tissues and materials are presented in Tables 1 and 2. Properties for the tumour were taken to be the same as for muscle, where it is seated, except for the blood perfusion rate and the metabolism which were both supposed to be zero.

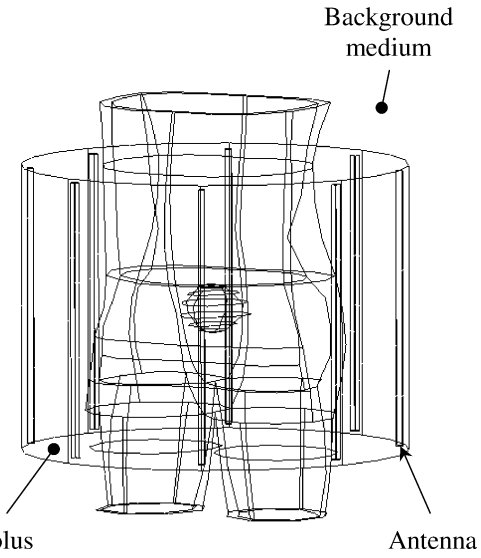

Fig. 2. Pelvic model enclosed within the Sigma-60 device.

Table 1
Tissue and material electrical properties at 100 MHz ($\varepsilon_0 = 8.854 \times 10^{-12}$ $F{\cdot}m^{-1}$, $\mu = \mu_0 = 4\pi \times 10^{-7}$ $H{\cdot}m^{-1}$) [14]

Tissue/material	$\varepsilon/\varepsilon_0$	σ
Fat	10.5	0.22
Muscle	72.0	0.889
Tumour	72.0	0.889
Water	78.0	0.0
Air	1.0	0.0

Table 2
Tissue thermal and thermophysical properties ($C_{pb} = 3475$ $J{\cdot}kg^{-1}{\cdot}K^{-1}$, $T_a = 37\,^{\circ}C$) [15]

Tissue	λ	W_b	Q_m
Fat	0.2	0.3	269.0
Muscle	0.545	0.433	703.5
Tumour	0.545	0.0	0.0

However, the effect on the temperature distribution caused by raising the tumour blood flow is also examined at the end of this section.

The capability of our optimisation method has been tested by considering two distinct configurations of the Sigma-60 heating device. In the first one, the electromagnetic parameters (amplitude and phase) of each antenna have been computed with the optimisation procedure described in Section 4. In the second one, no optimisation has been performed: all the amplitudes are the same and all the phases are set to zero, the common amplitude being adjusted in order to reach, at the centre of the tumour volume, the temperature obtained with the optimal configuration.

The results of the simulations with the optimised and non-optimised electromagnetic parameters are shown in Figs. 3 and 4, in terms of power deposition and temperature field. Note that the maximum temperature reached at the centre of

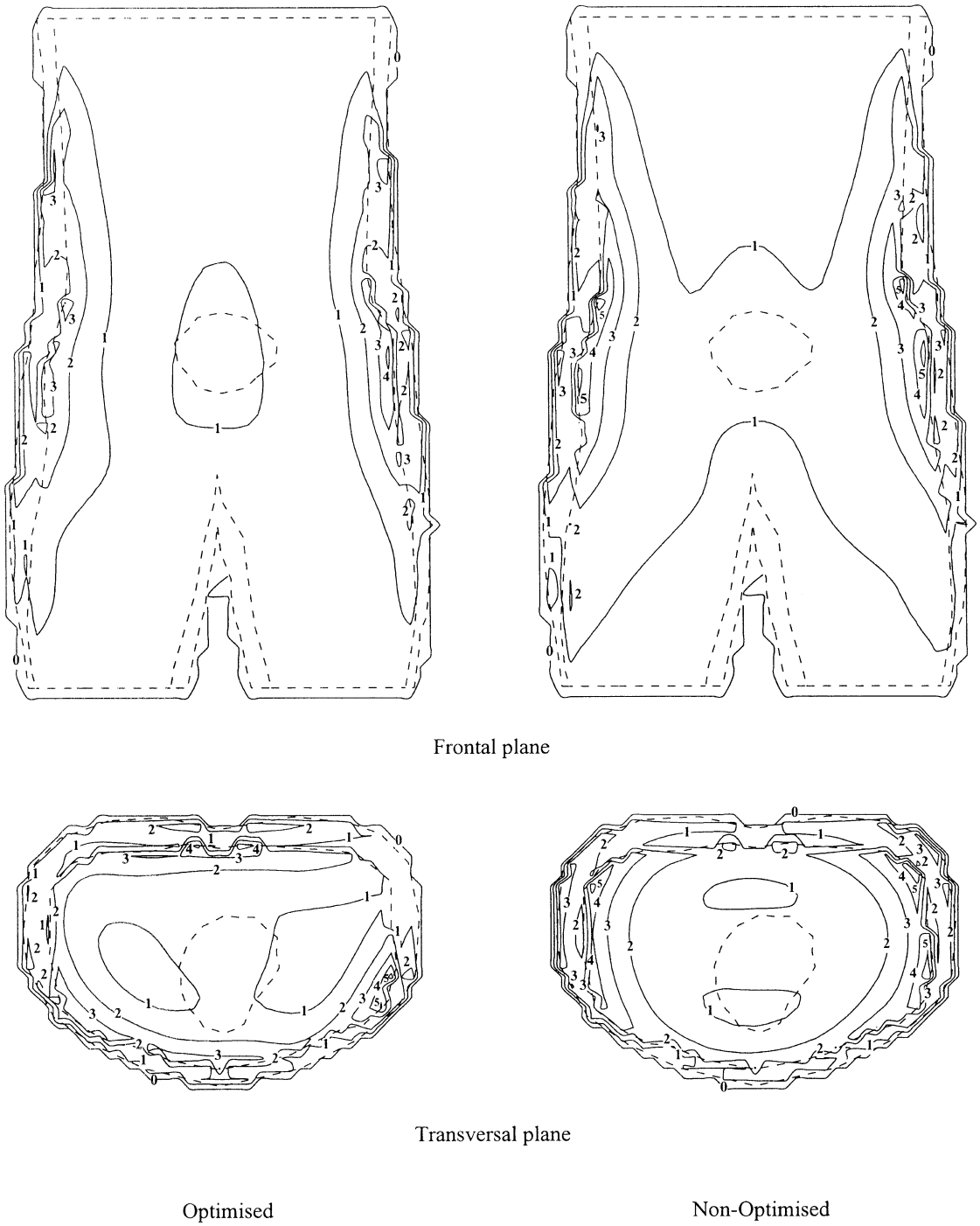

Fig. 3. Computed electromagnetic power deposition fields produced by the Sigma-60 heating device working at 100 MHz with optimised and non-optimised electromagnetic parameters. The visualisation planes cross the tumour at its centre and the dotted lines indicate the boundaries of different parts of the pelvic anatomical model. The scale is relative from 0 to 5 and the contour interval is 4000 $W \cdot m^{-3}$.

the tumour is about 44.9 °C. By examining the temperature patterns, one can notice that, with the two configurations, the heat deposition is well focused in the tumour and covers its entire volume. With the optimised set-up of the heating device, the temperature never exceeds 42 °C in the healthy tissues. On the contrary, the non-optimised case provides a dangerous overheating in two large areas localised in the muscle. Therefore, both the optimal and the non-optimal configurations lead to an efficient hyperthermia treatment of the tumour but only the optimal configuration provides a safe treatment. These conclusions clearly emphasise the contribution of our optimisation method. Besides, it is worth noting that no excessive heating of the superficial fat layer is observed. This comes from the cooling effect due to the water bolus. This comment is particularly important since the risk of overheating the superficial tissue constitutes

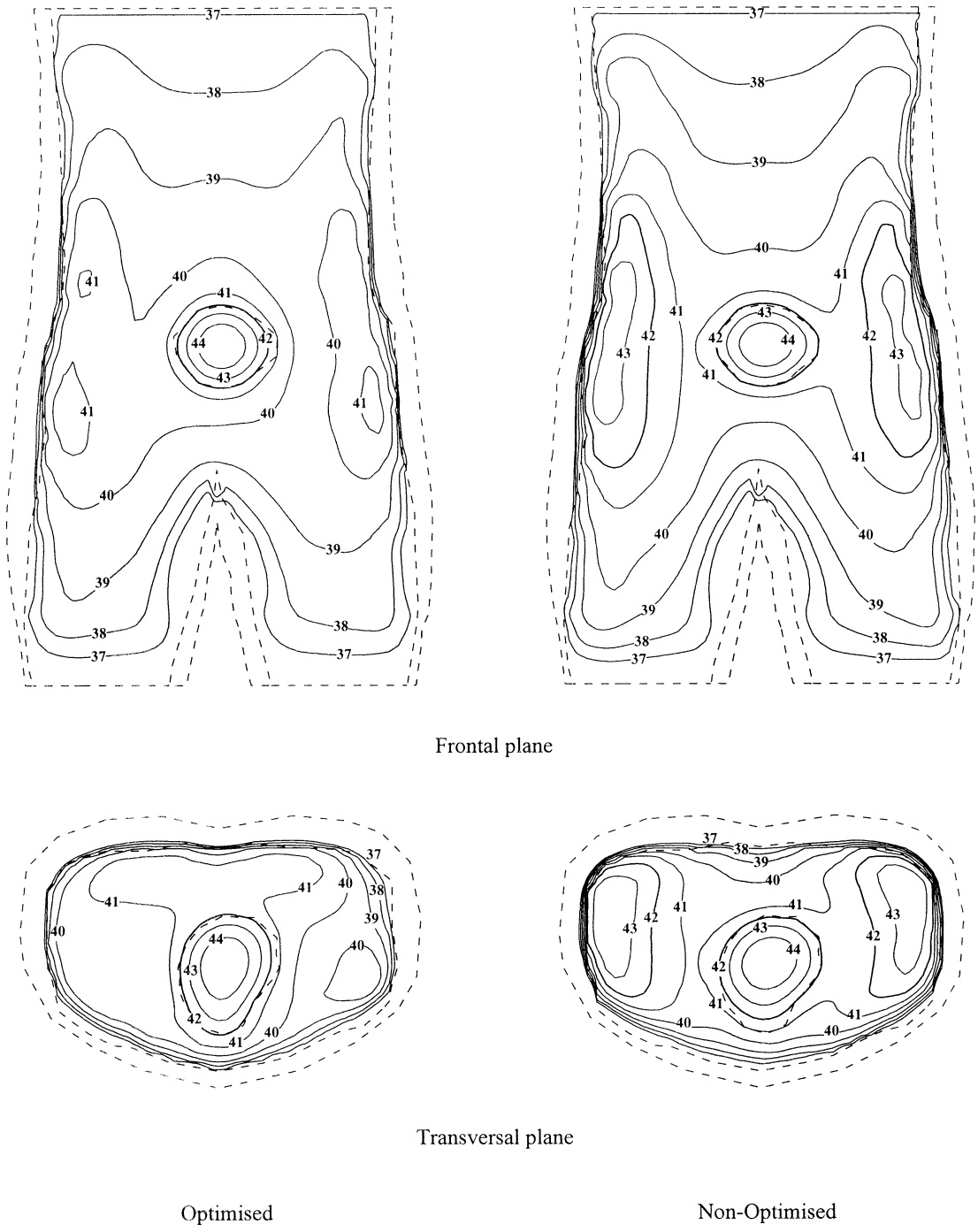

Fig. 4. Computed thermal fields (°C) produced by the Sigma-60 heating device working at 100 MHz with optimised and non-optimised electromagnetic parameters. Same visualisation planes as in Fig. 3.

a strong limiting factor in deep hyperthermia. As to the electromagnetic power deposition patterns with the optimal configuration, it can be pointed out that a large area around the tumour receives a non-negligible power. In addition to that, no particular focalisation over its volume is observed. Thus, our optimisation method can be actually distinguished from the ones involving a power deposition optimisation. With the non-optimal configuration, two high-absorbed power areas are created in the muscle leading to overheated areas in the healthy tissues. Besides, one can notice the discontinuities of the power deposition at the interface between the muscle and the fat. This fact, well-known in hyperthermia, comes from the abrupt change of electrical properties from one tissue type to another.

It is also interesting to evaluate the total power absorbed by the pelvic model. This power is about 213 W with the optimised electromagnetic parameters and about 242 W (12% increase) with the non-optimised ones. Therefore,

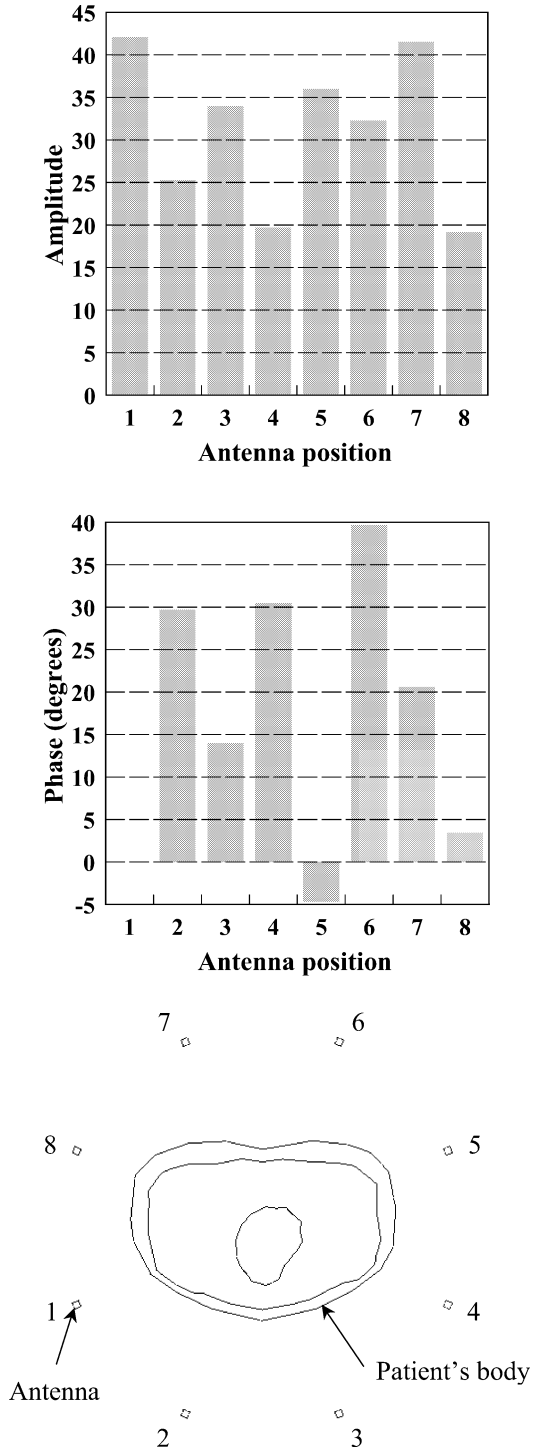

Fig. 5. Optimised electromagnetic parameters (amplitude and phase) of each antenna. The position of the antennas spaced around the patient's body is labelled from 1 to 8. The phase of the antenna in position 1 is set to zero.

the optimal configuration of the heating device produces an improved temperature distribution by requiring less power.

In Fig. 5 we have plotted the optimised parameters (amplitude and phase) of each antenna. The study of these values reveals that the optimal configuration deals with an intricate interplay among the electromagnetic sources. Thus,

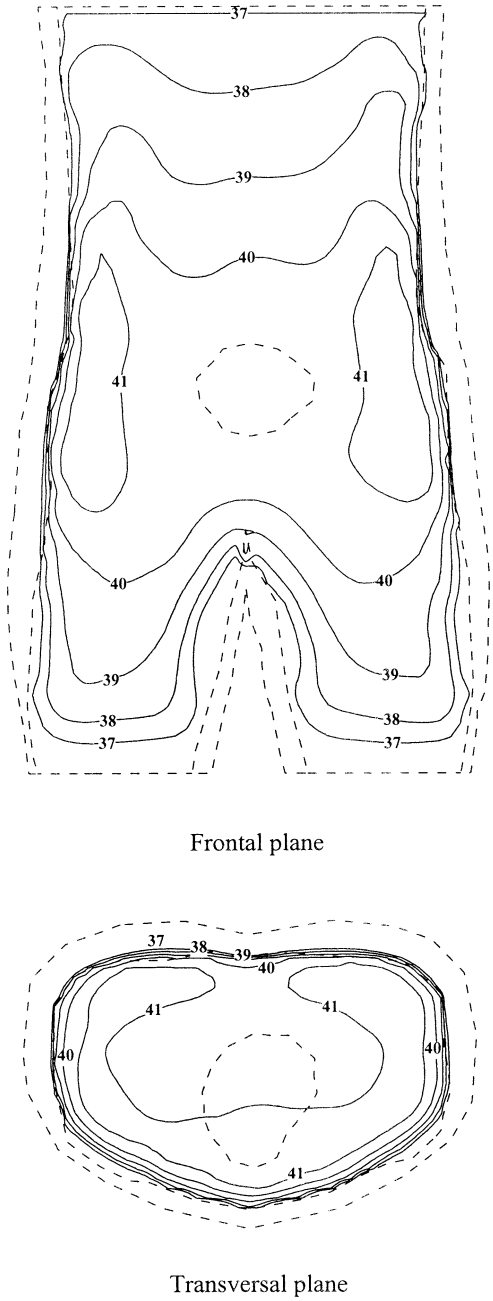

Fig. 6. Computed thermal fields (°C) produced by the Sigma-60 heating device working at 100 MHz with optimised electromagnetic parameters. The blood perfusion rate of the tumour is the same as for muscle. Same visualisation planes as in Fig. 3.

it appears to be difficult to estimate the suitable set of parameters without using appropriate optimisation tools.

To evaluate the influence of the tumour blood flow on the heating patterns, we have considered in the tumour a perfusion rate equivalent to that of the surrounding muscle. The thermal resulting fields computed with the optimised electromagnetic parameters are shown in Fig. 6. Clearly, temperature in the tumour tissue does not exceed 42 °C. Consequently, no therapeutic heating is achieved. This underlines the significant role of the tumour blood flow

in determining the efficiency of a hyperthermia treatment. Nevertheless, it is important to notice that the treatment provided is still safe since the temperature outside the tumour remains lower than 42 °C. Moreover, it is worth noting that some areas in the muscle are just below that level. So, there is no doubt that any trial of further raising the tumour temperature might lead to a dangerous treatment. It follows that our optimisation procedure plays correctly its role since it prevents from any overheating of the healthy tissues.

6. Conclusions

A three-dimensional model in heterogeneous media, based on the boundary element method, has been presented for solving the electromagnetic and the thermal problems that occur in the field of hyperthermia. Furthermore, an optimisation process, which tends to increase the concentration of heat over the tumour while keeping safe the surrounding tissues, has been developed. It breaks with the current trend to improve the power deposition only. This process is based on a superposition principle which applies first to the electromagnetic field and then to the temperature field. Thus, a set of elementary solutions can be computed once and for all (for each patient) and the optimal set-up of the heating device can be predicted without computing the whole electromagnetic and thermal problems at each trial. At last, three-dimensional simulations based on a rather realistic model of a person have been performed and have shown the potential of our method in regional hyperthermia treatment planning.

References

[1] P. Wust, M. Seebass, J. Nadobny, R. Felix, Electromagnetic deep heating technology, in: J.C. Bolomey, M.H. Seegenschmiedt, P. Fessenden, C.C. Vernon (Eds.), Thermoradiotherapy and Thermochemotherapy, Springer-Verlag, Berlin, 1995, pp. 219–251, Chapter 11.

[2] K.D. Paulsen, Principles of power deposition models, in: J.C. Bolomey, M.H. Seegenschmiedt, P. Fessenden, C.C. Vernon (Eds.), Thermoradiotherapy and Thermochemotherapy, Springer-Verlag, Berlin, 1995, pp. 399–423, Chapter 18.

[3] R.B. Roemer, Thermal dosimetry, in: M. Gautherie (Ed.), Thermal Dosimetry and Treatment Planning, Springer-Verlag, Berlin, 1990, pp. 119–214, Chapter 3.

[4] J. Mooibroek, J. Crezee, J.J.W. Lagendijk, Basics of thermal models, in: J.C. Bolomey, M.H. Seegenschmiedt, P. Fessenden, C.C. Vernon (Eds.), Thermoradiotherapy and thermochemotherapy, Springer-Verlag, Berlin, 1995, pp. 425–437, Chapter 19.

[5] C. Thiebaut, Modélisation tridimensionnelle du chauffage électromagnétique de tissus biologiques vivants. Application à la prédiction et à l'optimisation des effets de la thermothérapie, Ph.D. Thesis, Université de Poitiers, ENSMA, Poitiers, France, 2000.

[6] P.F. Turner, T. Schaefermeyer, BSD-2000 approach for deep local and regional hyperthermia: Clinical utility, Strahlenther. Onkol. 165 (1989) 700–704.

[7] P. Wust, M. Seebass, J. Nadobny, P. Deuflhard, G. Mönich, R. Felix, Simulation studies promote technological development of radiofrequency phased array hyperthermia, Internat. J. Hyperthermia 12 (1996) 477–494.

[8] K.D. Paulsen, S. Geimers, J. Tang, W.E. Boyse, Optimization of pelvic heating rate distributions with electromagnetic phased arrays, Internat. J. Hyperthermia 15 (1999) 157–186.

[9] S.K. Das, S.T. Clegg, T.V. Samulski, Electromagnetic thermal therapy power optimization for multiple source applicators, Internat. J. Hyperthermia 15 (1999) 291–308.

[10] C.A. Brebbia, J.C.F. Telles, L.C. Wrobel, Boundary Element Techniques—Theory and Applications in Engineering, Springer-Verlag, Berlin, 1984.

[11] J.A. Stratton, Electromagnetic Theory, McGraw-Hill, New York, 1941.

[12] J. Shen, Computational Electromagnetics Using Boundary Elements—Advances in Modelling Eddy Currents, Computational Mechanics Publications, Boston, 1995.

[13] C.A. Brebbia, On two different methods for transforming domain integrals to the boundary, in: C.A. Brebbia, J.J. Conner (Eds.), Advances in Boundary Elements, Vol. 1, Computational Mechanics Publications and Springer-Verlag, Berlin, 1989, pp. 59–74.

[14] D.R. Lynch, K.D. Paulsen, J.W. Strohbehn, Finite element solution of Maxwell's equations for hyperthermia treatment planning, J. Comput. Phys. 58 (1985) 246–269.

[15] Z.P. Chen, W.H. Miller, R.B. Roemer, T.C. Cetas, Errors between two- and three-dimensional thermal model predictions of hyperthermia treatments, Internat. J. Hyperthermia 6 (1990) 175–191.